RESEARCH ARTICLE



WILEY

Numerical simulation of unstable suction transients in unsaturated soils: the role of wetting collapse

Yanni Chen 🕒 | Giuseppe Buscarnera 🗅

Department of Civil and Environmental Engineering, Northwestern University, Evanston, Illinois, USA

Correspondence

Giuseppe Buscarnera, Department of Civil and Environmental Engineering, Northwestern University, Evanston, IL,

Email: g-buscarnera@northwestern.edu

Funding information

U.S. National Science Foundation, Grant/Award Number: ICER-1854951

Abstract

Fluid injection is one of the major triggering factors of instability in unsaturated soils. Robust simulation tools are therefore required to examine hydrologic transients in such a class of inelastic materials. In this paper, the governing equations imposing the balance of mass and momentum in deformable unsaturated porous media are inspected from an analytical perspective. Our main goal is to examine the role of volume collapse on the stability of suction transients. Distinct scenarios are considered in terms of material behavior, distinguishing the case of elastoplastic and viscoplastic materials. It shows that in elastoplastic materials the mathematical ill-posedness of the partial differential equations leads to a diffusive instability of the pore pressure field, signaled by the loss of stress controllability under water injection. By contrast, the introduction of viscosity restores the mathematical well-posedness and ensures the positive diffusivity. Numerical implications of these findings have been explored through simulations of water injection with a 1D finite element solver. It shows that an increase of the soil hydraulic sensitivity (i.e., a marked deterioration of the yield stress upon suction removal) can deteriorate the diffusive stability and prevent the computation of suction changes across a collapsible soil layer. While the incorporation of minor amounts of viscosity can restore numerical stability by suppressing the constitutive singularity. Such numerical results have been corroborated by the computation of local stability indicators based on controllability theory, which proved to be robust diagnostic tools to identify the culprit of runaway instability emerging from coupled hydro-mechanical processes.

KEYWORDS

diffusion processes, stability theory, unsaturated soils, viscoplasticity

INTRODUCTION

Water level fluctuations due to precipitation or rising phreatic levels are common triggers of ground failure. ^{1,2} The increase in moisture content and the consequent decrease in capillary suction weaken the soil and cause the accumulation of inelastic compaction, a phenomenon referred to as wetting collapse. As illustrated in Figure 1a, wetting may cause the accumulation of compactive strains, which can be replicated through concepts of strain-hardening plasticity.³ Large amounts of plastic compaction are known to deteriorate both the stability and the serviceability of systems subjected to wetting, possibly causing rapid ground movements and sudden acceleration (Figure 1b). Due to their detrimental consequences,

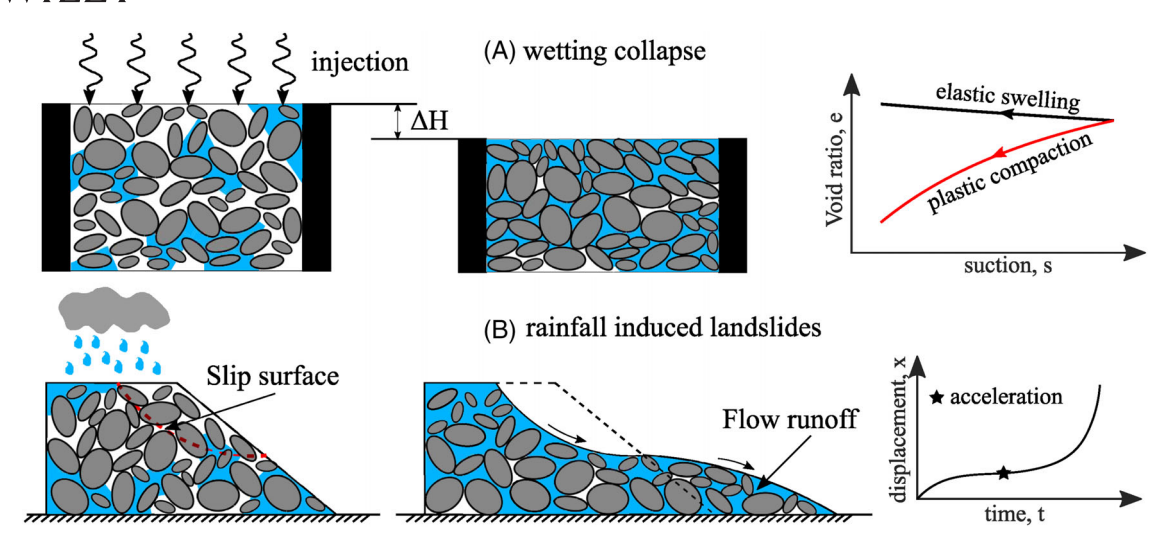


FIGURE 1 Schematic illustrations of wetting processes: (A) wetting collapse in laboratory tests. The schematic illustrates the different deformation outcomes of wetting simulations based on elastic models (resulting in swelling; black line) and plastic models with suction-dependent yield surface (which, instead, can replicate collapse mechanisms; red line); (B) rainfall induced landslides of the flow-type. The schematic illustrates the gradual transition from deceleration to acceleration with the star symbol signaling the emergence of global acceleration and runaway failure

numerous studies have been carried out to understand the mechanics of saturation-induced plastic deformation.^{4–6} For example, second-order work principles specific for unsaturated materials have been developed⁷ and linked to analytical tools to detect constitutive singularities in hydro-mechanical constitutive laws.⁸ In this context, constitutive singularities were linked to the concept of controllability, which provides indices to identify the onset of instability for very general combinations of control and response variables.^{9–11}

It is well known that material instability is a source of strain localization of rate-independent solids.^{12,13} Numerical implications of the post-failure responses are far-reaching and require the application of regularization strategies, such as viscoplasticity, gradient theory, and nonlocality.¹⁴ Similar concepts have also been explored in the context of fully saturated geomaterials, in which static liquefaction can lead to unstable consolidation processes.^{15–17} Usually, viscoplasticity is beneficial also for regularization of such ill-posed coupled hydro-mechanical processes.^{18,19} It is arguable that similar considerations remain valid also with reference to unsaturated porous media.^{6,20} However, to the authors' knowledge, no studies have yet documented explicitly the connection between the local instability associated with wetting-induced constitutive singularities and the numerical ill-posedness due to a vanishing diffusivity coefficient.

To fill this gap, this paper proposes an integrated analytical and numerical inspection of the field equations that govern coupled flow-deformation processes in collapsible unsaturated soils. By virtue of its known ability to suppress the ill-posedness caused by material instabilities, here, viscoplasticity is used to stabilize the numerical analyses of water diffusion in collapsible soils subjected to wetting. In the following sections, an analytical inspection of the governing equations is conducted for both elastoplastic and viscoplastic unsaturated materials, emphasizing the role of material inelasticity on the diffusive instability of pore pressure transients. It will be shown that although the diffusivity coefficient can be affected by the nonlinearity of the water retention behavior, viscosity restores its positiveness under very general choices of model parameters. In addition, such insights will be tested from a numerical standpoint by inspecting the characteristics of the discretized global stiffness matrix for both elastoplastic and viscoplastic constitutive formulations. More generally, the goal of the study is to illustrate the possibility to use a unified interpretation framework to track wetting-induced soil instability in coupled numerical analyses, as well as to suppress the numerical ill-posedness that results from them.

2 | DIFFUSIVE INSTABILITY OF UNSATURATED SOILS

2.1 | Mass conservation equation

Unsaturated porous media involve a solid phase permeated by two fluids, which are non-miscible and characterized by different affinity with the solid matrix (i.e., one of them is usually a wetting fluid capable of adhering to the matrix,

FIGURE 2 Schematic description of constitutive relationships to simulate wetting-induced inelastic deformation: (A) soil water retention curve (SWRC); (B) elastoplastic behavior in the σ -s space; (C) viscoplastic behavior with the overstress model in the σ -s space

while the other is a non-wetting fluid lacking such capability). Their mechanical behavior is governed by the interaction among these phases. Specifically, the fluids develop interfaces, across which a pressure jump is established. As a result, the pressure and consequent flow of the two fluids is controlled by independent variables and the interaction between the fluids and the matrix can be quantified by the pressure jump, here referred to as capillary suction. Although such conditions apply to multiple solid-fluid mixtures, hereafter emphasis is given to multiphase systems naturally occurring in the Earth, in which the solid matrix is represented by a quartz-based geomaterial skeleton (s), the wetting phase is pore water (w) and the non-wetting phase is air (a). The total volume V_t is then expressed as:

$$V_t = V_s + V_w + V_a \tag{1}$$

with the sum of V_w and V_a quantifying the volume of the voids, V_v . Void ratio, porosity, and degree of saturation are defined as $e = V_v/V_s$, $n = V_v/V_t$ and $S_r = V_w/V_v$ respectively, and the volume fractions of the three phases with respect to the total volume are expressed as 1 - n, nS_r and $n(1 - S_r)$, respectively. Moreover, suction quantifies the tendency of the pore water to possess pressure values lower than those prevailing in the air phase (i.e., $u_w < u_a$), and it is expressed as $s = u_a - u_w$. The relationship between suction, s, and degree of saturation, s, is described through the water retention behavior. The stress acting on the solid skeleton can be quantified by the so-called Bishop effective stress:

$$\sigma'_{ij} = \sigma^{\text{net}}_{ij} + \chi(S_r) s \delta_{ij}$$
 (2)

where δ_{ij} is the Kronecker delta, $\sigma_{ij}^{\rm net} = \sigma_{ij} - u_a \delta_{ij}$ is the net stress, σ_{ij} is the total stress, and $\chi(S_r)$ is the effective stress coefficient, being a function of S_r . In addition, the analysis is restricted to moderate values of S_r , reflecting of materials within the funicular regime²¹ for which both water and air phases are continuous and the air pressure can be considered constant (i.e., $\dot{u}_a = 0$), as shown in Figure 2a. Therefore, only the mass balance of water is hereafter considered:

$$\left(\rho_w q_i^w\right)_{,j} + \left(\rho_w n S_r\right)_{,t} = 0 \tag{3}$$

where commas indicate differentiation with respect to either time (i.e., $\partial a/\partial t = a_{,t}$) or a spatial coordinate (e.g., $\partial a/\partial x = a_{,x}$ and $\partial^2 a/\partial x^2 = a_{,xx}$). Subscripts i and j indicate spatial directions within a Cartesian reference system through indicial notation and follow the Einstein summation convention. q_i^w is the water flux following Darcy's law:

$$q_{i}^{w} = -k_{ij}^{w} h_{,j} = -k_{ij}^{w} \left(-\frac{s}{\gamma_{w}} + z \right)_{,j}$$
(4)

where γ_w is the specific weight of water, h is the hydraulic potential, here contains the contributions of the pressure potential $-s/\gamma_w$ and the gravitational potential z, and $k_{ij}^w(S_r)$ is the hydraulic conductivity tensor associated to S_r . Specifically, under the small strain assumption, the Lagrangian porosity is adopted here²² which implies that $n = e/(1 + e_0)$, where e_0 is the initial void ratio, and $n_{,t} = -\varepsilon_{v,t}$, where ε_v is the volumetric strain. By adopting the compression positive sign

convention typical for geomechanical analyses, it follows:

$$(nS_r)_{,t} = nS_{r,t} - S_r \varepsilon_{v,t} = \frac{e_{w,t}}{1 + e_0}$$
 (5)

where $e_w = eS_r$ is the specific water ratio, defined as the product of void ratio, e, and degree of saturation, S_r . By treating the water phase as incompressible (i.e., water density ρ_w keeps constant), the governing equation for water mass balance defined in Equation 3 becomes:

$$q_{i,j}^w + \frac{e_{w,t}}{1+e} = 0 ag{6}$$

Combining with Equation (4) leads to:

$$\frac{k_{ij}^{w}}{\gamma_{w}} s_{,ij} + \frac{1}{\gamma_{w}} \frac{\partial k_{ij}^{w}}{\partial s} s_{,i} s_{,j} - k_{ij,i}^{w} z_{,j} + \frac{e_{w,t}}{1+e} = 0$$
 (7)

Moreover, the hypothesis of additive strain decomposition enables to express the total strain ε_{ij} as the sum of elastic and plastic portions, $\varepsilon_{ij}^{\varrho}$ and ε_{ij}^{p} , respectively. By incorporating an uncoupled water retention curve (i.e., a unique relationship between suction and degree of saturation), it follows:

$$\frac{e_{w,t}}{1+e} = n \frac{\partial S_r}{\partial s} s_{,t} - S_r \left[C_{ijkl}^e \left(\sigma_{ij,t}^{\text{net}} + \frac{\partial \sigma_{ij}'}{\partial s} s_{,t} \right) \delta_{kl} + \varepsilon_{ij,t}^p \delta_{ij} \right]$$
(8)

where C^e_{ijkl} is the elastic compliance tensor, the inverse of the elastic stiffness matrix D^e_{ijkl} . While the derivations above do not encompass changes of water retention capacity due to volume strains, ^{23,24} it has been shown that the role of such further coupling effects does not lead to major alterations of the mathematical tools necessary to diagnose wetting instabilities. ¹⁰ The formalism of plastic strain increments relies on the adopted flow rule which differentiates between elastoplasticity and viscoplasticity.

2.2 | Diffusive instability of elastoplastic materials

Within the framework of elastoplasticity, the flow rule is generalized as:

$$\varepsilon_{ij,t}^{p} = \Lambda \frac{\partial g}{\partial \sigma_{ij}'} \tag{9}$$

where g is the plastic potential function; Λ is the plastic multiplier derived from the consistency condition, which guarantees the stress state keeping on or within the yield surface as shown in Figure 2(B):

$$\frac{\partial f}{\partial \sigma'_{ij}} \sigma'_{ij,t} + \frac{\partial f}{\partial \sigma_y} \sigma_{y,t} = 0 \tag{10}$$

in which σ_y is the internal variable quantifying the size of yield function f and it is normally governed by a hydromechanical hardening law expressing as^{4,25}:

$$\sigma_{y,t} = \frac{\partial \sigma_y}{\partial \varepsilon_{ij}^P} \varepsilon_{ij,t}^P + \frac{\partial \sigma_y}{\partial s} s_{,t} \tag{11}$$

By inserting Equations (2) and (11) into Equation (10), Λ is derived as:

$$\Lambda = \frac{1}{H} \left[\frac{\partial f}{\partial \sigma'_{ij}} \sigma_{ij,t}^{\text{net}} + \left(\frac{\partial f}{\partial \sigma'_{ij}} \frac{\partial \sigma'_{ij}}{\partial s} + \frac{\partial f}{\partial \sigma_{y}} \frac{\partial \sigma_{y}}{\partial s} \right) s_{,t} \right], \quad H = -\frac{\partial f}{\partial \sigma_{y}} \frac{\partial \sigma_{y}}{\partial \varepsilon_{ij}^{p}} \frac{\partial g}{\partial \sigma'_{ij}}, \tag{12}$$

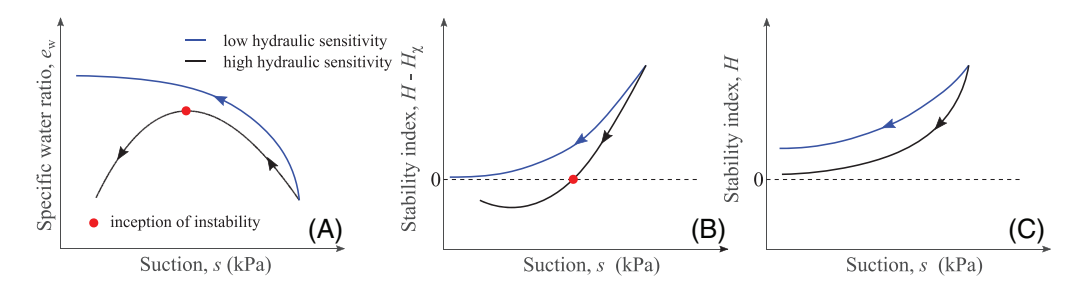


FIGURE 3 Schematics of wetting instability due to water injection: (A) material response in the s- e_w space; (B) evolution of the elastoplastic stability index

Combining Equations (7), (8), (9), and (12), the diffusive equation of the transient flow can be compacted into a parabolic partial differential equation (PDE):

$$\frac{k_{ij}^{w}}{\gamma_{vv}} s_{,ij} - C_1 s_{,t} + C_2 \left(s_{,i}, \sigma_{ij,t}^{\text{net}} \right) = 0$$
(13)

where the coefficient C_1 is expressed as:

$$C_{1}^{ep} = -\frac{B}{H}(H - H_{\chi})$$

$$B = n\frac{\partial S_{r}}{\partial s} - S_{r}C_{ijkl}^{e}\frac{\partial \sigma_{ij}'}{\partial s}\delta_{kl}, H_{\chi} = \frac{S_{r}}{B}\left(\frac{\partial f}{\partial \sigma_{ij}'}\frac{\partial \sigma_{ij}'}{\partial s} + \frac{\partial f}{\partial \sigma_{y}}\frac{\partial \sigma_{y}}{\partial s}\right)\frac{\partial g}{\partial \sigma_{ij}'}\delta_{ij}$$
(14)

Note that the superscript "ep" in C_1 indicates the use of elastoplasticity and is meant to distinguish the term in Equation (14) from those which will be derived with reference to viscoplastic constitutive relations (for which the superscript "vp" will be employed).

From a mathematical standpoint, the stability of the parabolic PDE in Equation (13) is ensured when ²⁶:

$$C_1 > 0 \tag{15}$$

Violations of such condition render the differential problem ill-posed, thus opening the possibility for unstable pore pressure fields. Specifically, for elastoplastic materials, the positiveness of C_1^{ep} is controlled by the sign of terms B, H, and $H-H_\chi$. Term B depends on the definition of $\chi(S_r)$ and the water retention behavior, here, it simply assumes $\chi(S_r) = S_r$ although numerous expressions have been suggested for $\chi(S_r)$. Then, term B can be expressed as:

$$B = S_r \frac{\partial S_r}{\partial s} \left(\frac{n}{S_r} - \frac{s \delta_{ij} \delta_{kl}}{D_{ijkl}^e} - \frac{S_r \delta_{ij} \delta_{kl}}{D_{ijkl}^e} \frac{\partial s}{\partial S_r} \right)$$
(16)

Normally, in geomaterials, the values of porosity and degree of saturation have the same order of magnitude, while capillary suction levels relevant for collapse phenomena are usually a few orders of magnitude lower than the value of elastic stiffness. This argument implies that the contribution of $s\delta_{ij}\delta_{kl}/D^e_{ijkl}$ in Equation 16 is negligible compared to term n/S_r . Furthermore, according to the water retention characteristics, $\partial S_r/\partial s$ or $\partial s/\partial S_r$ always takes negative values, implying that term B can be regarded as negative. By contrast, the signs of H and $H-H_\chi$ are associated with the loss of controllability under mixed hydro-mechanical controls. Specifically, H coincides with the stability index H defined for wetting tests conducted under constant stress and prescribed suction (i.e., $\sigma^{\rm net}_{ij,t}=0$ and the prescribed s_t), while $H-H_\chi$ being the stability index H customized for wetting tests conducted under constant stress and prescribed water mass injection (i.e., $\sigma^{\rm net}_{ij,t}=0$ and the prescribed $e_{w,t}$), as shown in Appendix A1. As illustrated in Figure 3, the occurrence of non-positive values of $H-H_\chi$ always precedes non-positive values of H, which normally remains positive throughout the wetting stage. Therefore, the sign of C_1^{ep} would primarily depend on the sign of term $H-H_\chi$, with its negativeness indicating a loss of material stability during water injection and the singularity of the constitutive operator. The transition of

 $H-H_\chi$ from positive to negative values corresponds to a peak in e_w , which implies a state at which the specimen has a spontaneous tendency to expel large volumes of fluid through collapse deformation, thus being unable to sustain an arbitrary volume of injected fluid. Such findings illustrate that wetting-induced instability at the material point level has the ability to cause diffusive instability, thus leading to potentially detrimental consequences on the robustness of coupled hydro-mechanical simulations.

2.3 | Diffusive instability of viscoplastic materials

Elastoplastic constitutive equations can be readily converted to a viscoplastic form through the strategy proposed by Perzyna^{30,31}, which enables the state of stress to violate the consistency condition. The amount of such violation is quantified through the so-called overstress f, that is, a measure of the distance between the current stress state and yield surface (Figure 2C). The overstress is directly used to feed a viscoplastic flow rule, defined as:

$$\varepsilon_{ij,t}^{vp} = \phi(f,\eta) \frac{\partial g}{\partial \sigma'_{ij}},\tag{17}$$

where η is the viscosity and ϕ is the viscous nucleus function. After combining it with Equations (7) and (8), the coefficient C_1 specified for viscoplastic materials is expressed as:

$$C_1^{vp} = -B > 0 \tag{18}$$

The positiveness of the diffusive coefficient C_1^{vp} implies that the introduction of viscosity can suppress the diffusive instability regardless of the material response, thus offering the possibility to develop more robust numerical tools to study hydro-mechanical coupled processes in the post-instability regime.

3 | NUMERICAL IMPLEMENTATION

To numerically inspect the effectiveness of the above findings, field equations governing the coupled hydromechanical process for elastoplastic and viscoplastic unsaturated porous media are discretized and solved through the finite element (FE) approach. Following the standard procedure of FE discretization, equation systems describing the hydromechanical process can be condensed as follows:

$$\mathbf{A}\dot{\mathbf{X}} + \mathbf{B}\mathbf{X} = \mathbf{R} \tag{19}$$

in which:

$$\mathbf{A} = \begin{bmatrix} \mathbf{K} & \mathbf{L} \\ \mathbf{L}' & \mathbf{W} \end{bmatrix}, \mathbf{B} = \begin{bmatrix} \mathbf{0} & \mathbf{0} \\ \mathbf{0} & \mathbf{H} \end{bmatrix}, \mathbf{R} = \begin{bmatrix} \dot{\mathbf{F}}_{\text{ext}} \\ \dot{\mathbf{Q}}_{\text{ext}} \end{bmatrix}, \dot{\mathbf{X}} = \begin{bmatrix} \dot{\mathbf{U}} \\ \dot{\mathbf{P}} \end{bmatrix}, \mathbf{X} = \begin{bmatrix} \mathbf{U} \\ \mathbf{P} \end{bmatrix}$$
(20)

where the coefficient matrices differ between elastoplastic and viscoplastic materials due to the different treatment of the inelastic effects as detailed in Appendix A2. Specifically, for elastoplasticity, the plastic deformations directly impact the global stiffness matrix \mathbf{K} , while for viscoplasticity, the global stiffness matrix is affected only by the elastic properties with the inelastic effects collected into a pseudo-forcing term $\dot{\mathbf{F}}_{\text{ext}}^{ps}$ contributing to the total forcing agent $\dot{\mathbf{F}}_{\text{ext}}$. Such major difference provides further insight explaining why viscous regularization can be an effective strategy to suppress the ill-posedness of diffusive equations. To numerically solve the coupled nonlinear system, an explicit integration scheme enhanced with adaptive time-stepping and automatic error control^{32,33} has been implemented. In addition, a higher degree of interpolation for the displacement field was used with respect to the pore pressure field to guarantee further robustness. Specifically, in the simulations that follow three-node elements are used for the displacement field and two-node elements for the pore pressure field. A validation example of the numerical implementation is provided in Appendix A3 with reference to the Liakopoulos drainage test.

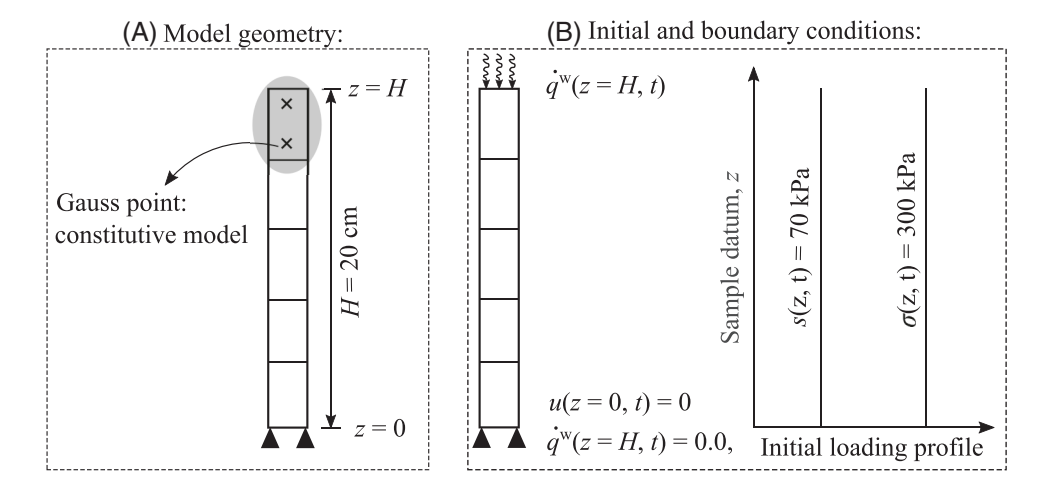


FIGURE 4 Schematic description of the numerical example: (A) model geometry; (B) initial and boundary conditions. *H* is the sample height, t is time, and z is the datum

4 | SIMULATION OF WETTING-INDUCED COLLAPSE IN 1D SOIL COLUMNS

4.1 | Problem description

A 1D unsaturated soil column is used to illustrate, from a numerical standpoint, the connection between material instability and the ill-posedness of the diffusive processes caused by water injection. In addition, the analyses are meant to test the effectiveness of viscoplastic regularization for coupled infiltration-deformation problems involving collapsible unsaturated geomaterials. As detailed in Figure 4, a homogeneous soil column with a height of 20 cm is employed. The column is subjected to a constant axial stress $\sigma = 300$ kPa applied at the top and an initially uniform suction profile with s = 70 kPa (i.e., the contribution of the body force is assumed negligible). Water is injected through the top surface at a constant rate while fixing the displacement and preventing drainage at the bottom. The simple 1D constitutive model²⁵ detailed in the following section is used to simulate wetting-induced plastic compaction. Two testing scenarios are performed by using materials with low and high hydraulic sensitivity (here reflected by the parameter r_{sw}) to obtain a stable and an unstable case, respectively.

4.2 | Model specification

The simple 1D constitutive relationship is used in this work with the linear elasticity:

$$\sigma_t' = E\varepsilon_t^e \tag{21}$$

where *E* represents the Young's modulus. The yield condition is defined as:

$$f = \sigma' - \sigma_{\gamma} \tag{22}$$

Given the one-dimensional nature of the selected constitutive description, the flow rule can be regarded as associated (i.e., f = g). Although this is a strong approximation for geomaterials, the benefit of this simplification is to suppress all possible sources of material instability other than the suction-induced deterioration of the yielding conditions. The latter effect is reproduced mathematically through the following hydro-mechanical hardening law⁴:

$$\sigma_{y,t} = \frac{\sigma_y}{B_p} \varepsilon_{,t}^p - r_{sw} \sigma_y S_{r,t} \tag{23}$$



TABLE 1 Summary of model parameters and loading conditions

test type	E [kPa]	\boldsymbol{B}_p	r_{sw}	$a_v g$	$m_v g$	$n_v g$	$k^{\rm sat}$ [cm/h]	μ[1/h]	\dot{q}^w [cm/h]
stable	5000	0.7	1.4	0.17	0.31	1.13	1.0	1000	4.0
unstable	5000	0.7	2.0	0.17	0.31	1.13	1.0	1000	0.52

where B_p is the hardening parameters and r_{sw} quantifies the hydraulic sensitivity, with higher values indicating a stronger effect of suction on the expansion/contraction of the elastic domain. Here, only one internal variable accounting for the yielding threshold is considered, a typical assumption used in the constitutive modeling of geomaterials.

According to Equations 12 and 14, the stability index $\mathcal{H} = H - H_{\gamma}$ can be expressed as:

$$H = \frac{\sigma_y}{B_p}, \quad H_\chi = \frac{S_r}{B} \left(S_r + s \frac{\partial S_r}{\partial s} + r_{sw} \sigma_y \frac{\partial S_r}{\partial s} \right)$$

$$B = n \frac{\partial S_r}{\partial s} - \frac{S_r^2}{E} - \frac{sS_r}{E} \frac{\partial S_r}{\partial s} < 0$$
(24)

Since B generally takes a negative value (detailed in Section 2), the increase in r_{sw} brings positive contributions to H_{χ} which deteriorates the stability condition and leads to unstable responses. In other words, higher r_{sw} increases the weakening effect due to an increase of the degree of saturation and causes unstable wetting collapse as illustrated in Figure 3.²⁹

The extension of the constitutive law detailed above to viscoplasticity requires the definition of an additional function controlling the magnitude of the strain rate, referred to as viscous nucleus:

$$\phi = \mu \frac{f}{\sigma_y} \tag{25}$$

where μ is a fluidity (the inverse of viscosity, η) and f quantifies the magnitude of the overstress. The selected formulation can be regarded as a particular example of Bingham-type model and reduce automatically to its elastoplastic counterpart for high values of fluidity, μ . As to the hydraulic features, the Van Genuchten water retention curve (SWRC)³⁸ is adopted:

$$S_r = \left[1 + \left(a_{vg}s\right)^{n_v g}\right]^{-m_{vg}} \tag{26}$$

where a_{vg} , m_{vg} and n_{vg} are shape parameters. And the Mualem's equation³⁹ is used to describe the impact of S_r on the hydraulic conductivity, k_w :

$$k_w = k_w^{\text{sat}} \sqrt{S_r} \left[1 - \left(1 - S_r^{1/m_{vg}} \right)^{m_{vg}} \right]^2$$
 (27)

where $k_w^{\rm sat}$ is the hydraulic conductivity at saturated conditions. Here, the wetting-collapse simulations are performed in idealized soil systems characterized by different values of hydraulic sensitivity, thus examining the numerical implications of various types of wetting-collapse behaviors. Table 1 lists the model parameters and injection rates for the two proposed cases.

4.3 | Model performance

Figure 5 shows the simulation results of the wetting test on a simulated material with low hydraulic sensitivity (i.e., $r_{sw} = 1.4$). The results are illustrated with reference to both elastoplastic and viscoplastic constitutive laws. Specifically, although soils generally shows viscous responses, ^{40,41} here, the introduction of viscosity is mainly aimed at regularizing the numerical analyses and enabling the investigation of the post-instability regime. For this reason, a minor amount of viscosity ($\eta = 10^{-3}$ h) is used to limit the viscous effect on material responses at the stable regime while restoring the mathematical well-posedness after instability. As indicated by Figure 5(B), the sample is not saturated instantaneously throughout the volume, but it displays time-dependent patterns due to the relatively low permeability. The Gauss points

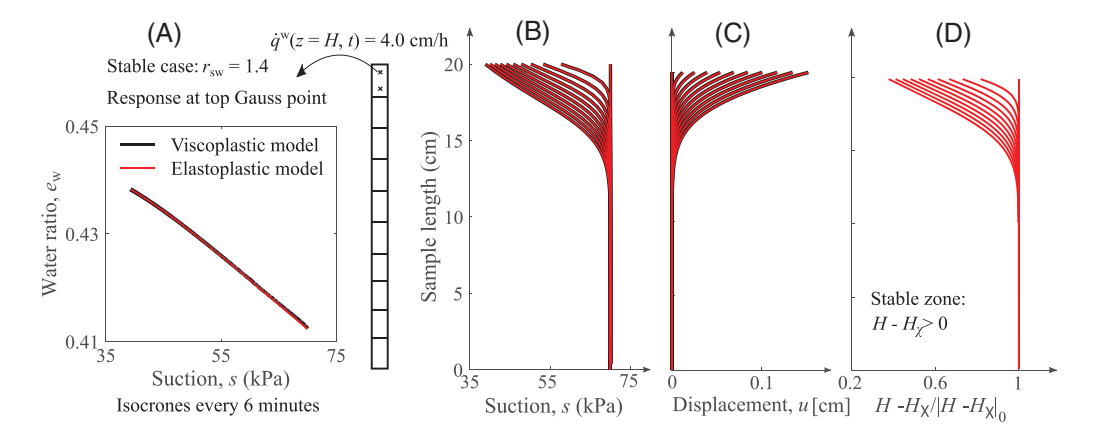


FIGURE 5 Simulation of the stable injection test with elastoplastic and viscoplastic models on low hydraulic sensitivity samples $r_{sw} = 1.4$: (A) the s- e_w relationship at the top Gauss point; (B,C) 6-min isochrones of nodal displacement and suction; (D) 6-min isochrones of elastoplastic stability index at Gauss points

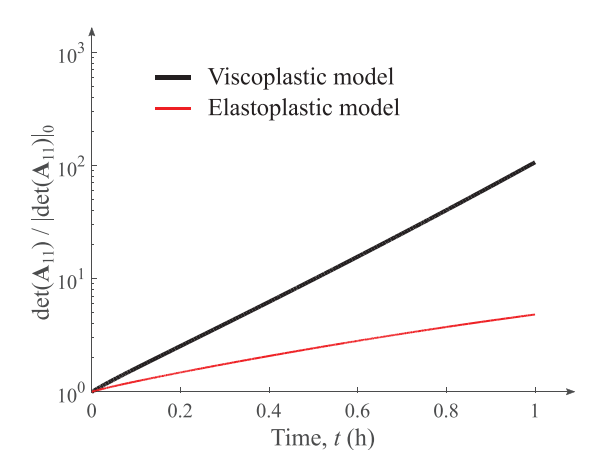


FIGURE 6 Time evolution of the global stability index for the stable injection test

near the top of the column are saturated first and experience a higher suction drop, while as the water gradually flows downwards, other parts of the sample start to saturate. For this reason, Figure 5(A) inspects the relationship between s and e_w for the top Gauss point and a stable process without the onset of a peak response is observed. Figure 5(d) shows that the stability index $H - H_\chi$ is positive at all Gauss points during the wetting process. Figure 5(A-C) illustrates a nearly perfect overlap between the elastoplastic and viscoplastic responses, which verifies that the introduction of slight viscosity has negligible influence on the model prediction for stable cases. Furthermore, the well-posedness of the numerical problem is indicated by the positiveness of the determinant of the discretized global operator \mathbf{A} (i.e., Equation 20) condensed by taking into account the boundary conditions, $^{42-44}$ which involves the partition of the coefficient matrix \mathbf{A} to separate the components associated to the Dirichlet boundaries, being:

$$\mathbf{A} = \begin{bmatrix} \mathbf{A}_{11} \ \mathbf{A}_{12} \\ \mathbf{A}_{21} \ \mathbf{A}_{22} \end{bmatrix} \tag{28}$$

where A_{11} corresponds to the nodal fields independent of the Dirichlet boundaries. Thus, numerical stability is quantified by det A_{11} , which keeps positive for the stable case as displayed in Figure 6.

Figure 7 shows the simulation results of the wetting test on a material with higher hydraulic sensitivity (i.e., $r_{sw} = 2.0$). The onset of wetting instability, marked by the transition of stability index $H - H_{\chi}$ from positive to negative values as shown in Figure 7(d), initially occurs at the top Gauss point and propagates downwards. As proved theoretically, the local failure of elastoplastic materials is capable to trigger the onset of numerical instability and cause the breakdown of the FE analysis. Figure 7(A) compares the response at the top Gauss point with a material point simulation under similar

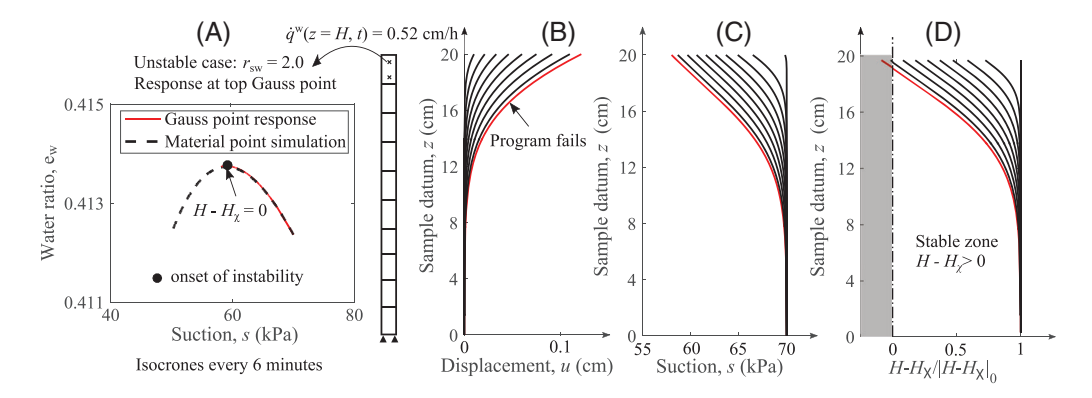


FIGURE 7 Simulation of the unstable injection test with the elastoplastic model on high hydraulic sensitivity samples $r_{sw} = 2.0$: (A) the s- e_w relationship at the top Gauss point; (B,C) 6-minute isochrones of nodal displacement and suction; (D) 6-minute isochrones of material stability index at Gauss points

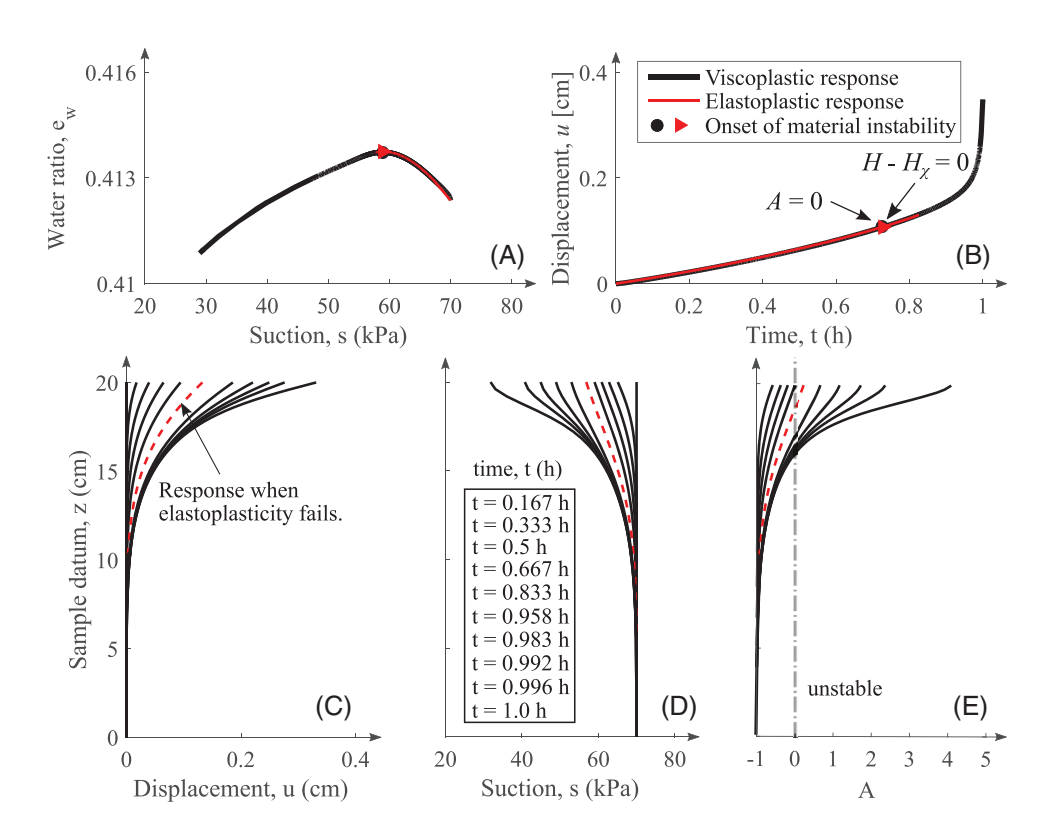


FIGURE 8 Simulation of the unstable injection test with the viscoplastic model on high hyraulic senstitivity samples $r_{sw} = 2.0$: (A) comparison of the s- e_w relationship at the top Gauss point between elastoplastic and viscoplastic model; (B) comparison of surface displacement between elastoplastic and viscoplastic model; (C,D) 6-min isochrones of nodal displacement and suction; (E) 6-min isochrones of stability index at Gauss points

constraints (i.e., wetting test under fixed mechanical loading). Such comparison illustrates that prior to instability the two simulations display close agreement, but the FE analysis with elastoplasticity fails right after the onset of material instability and prevents the continuation of the numerical analysis within the immediate post-peak regime. It is worth noting that control conditions imposed at the material point level are chosen in such a way to bypass the constitutive singularity (i.e., suction is directly controlled, thus guiding the intensity of material deterioration), while the boundary conditions in the numerical simulation involve directly water injection, thus implying that the amount of suction variation throughout the domain is an outcome of both the local material response and the global system response.

To check the effects of viscoplastic regularization, the same analysis is repeated with the viscoplastic model counterpart. Figure 8(A) and (B) compare the simulation results of elastoplastic and viscoplastic models, while Figure 8(c) and (d)

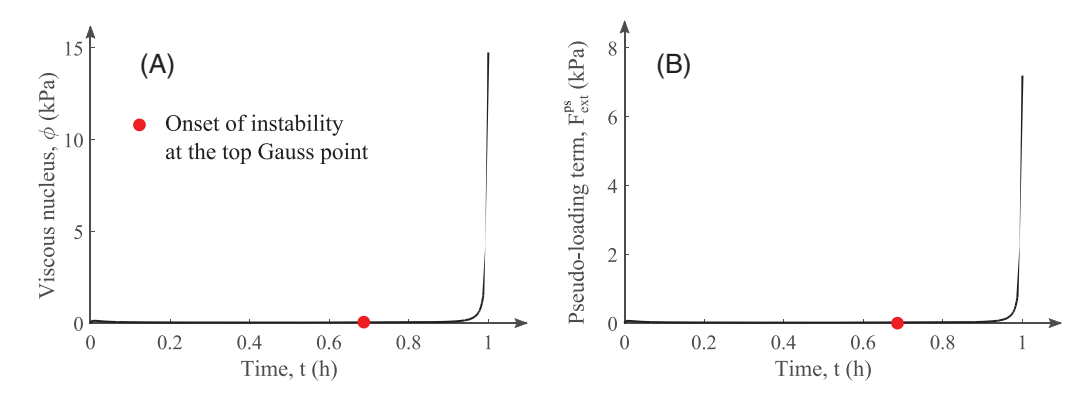


FIGURE 9 Simulation of the unstable injection test with the viscoplastic model: (A) time history of the viscous nucleus function ϕ at the top Gauss point; (B) time history of the pseudo-loading term at the top node F_{evt}^{ps}

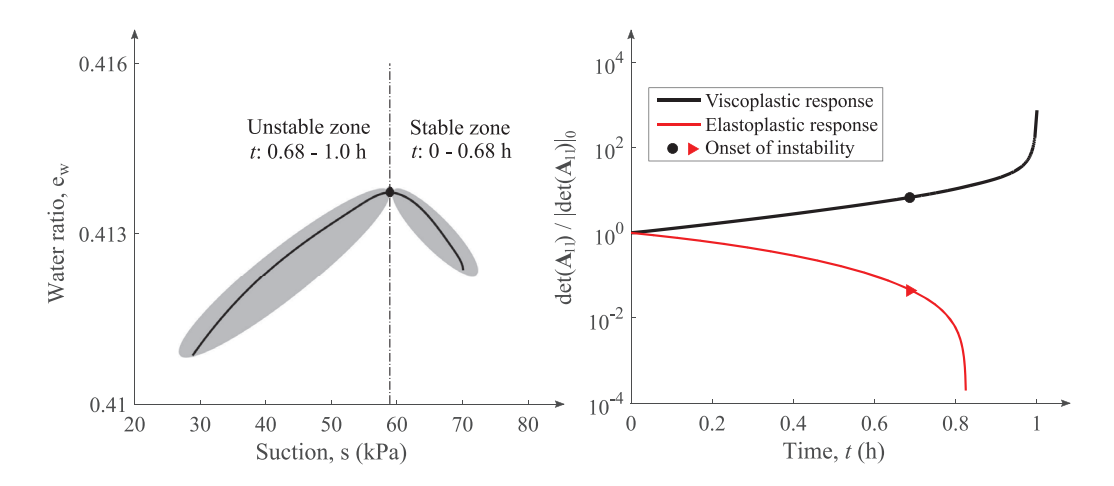


FIGURE 10 Simulation of the unstable injection test: (A) s- e_w relationship at the top Gauss point simulated with the viscoplastic model before and after the onset of instability; (B) time history of the global stability index for both elastoplastic and viscolpastic models

present the nodal displacement and suction profile of the viscoplastic simulation. The results readily show that prior to instability the computations obtained with the two models match perfectly. However, the introduction of viscosity can effectively suppress the numerical instability and continue the simulation within the post-peak regime. The initial stages leading to an impending runaway response are signaled by the abrupt displacement acceleration and rapid suction loss, which is mathematically quantified by the vanishing of the viscous stability index, A, proposed by 25 for suction-dependent viscoplastic models as shown in Figure 8(e) (see Appendix A4 for more details). It implies that although the constitutive instability of the viscoplastic material does not lead to a numerical ill-posedness, it still represents a precursor of the unstable temporal evolution of suction and strain across the domain, which is another form to express the occurrence of a system instability triggered by a rapidly growing forcing agent $F_{\rm ext}^{\rm vp}$, whose sharp evolution is a direct consequence of the values of the viscous nucleus function (Figure 9).

Figure 10(A) further details the stable and unstable portion of the s- e_w relationship for viscoplastic modeling on high hydraulic sensitivity samples, where it is shown that suction changes more rapidly during the unstable process. Figure 10(B) examines instead the evolution of numerical stability index marked by $\det \mathbf{A}_{11}$ for elastoplastic and viscoplastic models, for which the transition from positive to negative indicates the potential occurrence of numerical instability for boundary value problems due to the singularity of the discretized global operator. As indicated in Figure 10(B), it decreases steadily to zero until the elastoplastic analysis stops abruptly, while contrarily, it increases during the viscoplastic simulation. This provides additional evidence to mathematically support how viscosity contributes to regularize the numerical instability.

Furthermore, the introduction of viscosity also brings time-dependency to the material response in addition to permeability, which is crucial to enrich the understanding of delayed failures widely observed in nature⁴⁶ and explore the system evolution after the occurrence of wetting-induced instability. In this context, a suction-controlled creep phase is

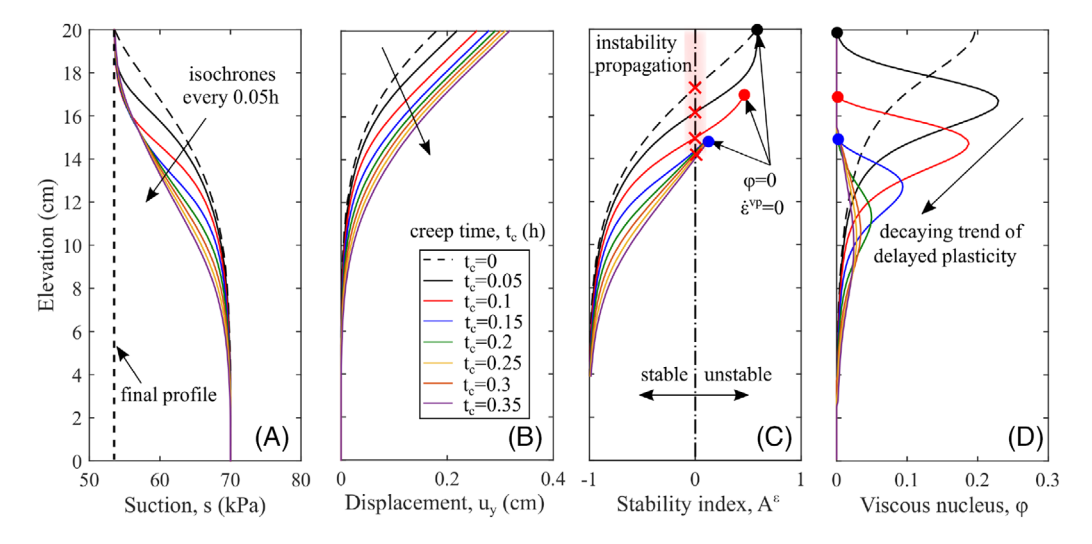


FIGURE 11 Isochrones of creep responses every 0.05 h under constant suction at the top surface: (A) suction; (B) displacement; (C) stability index; (D) viscous nucleus

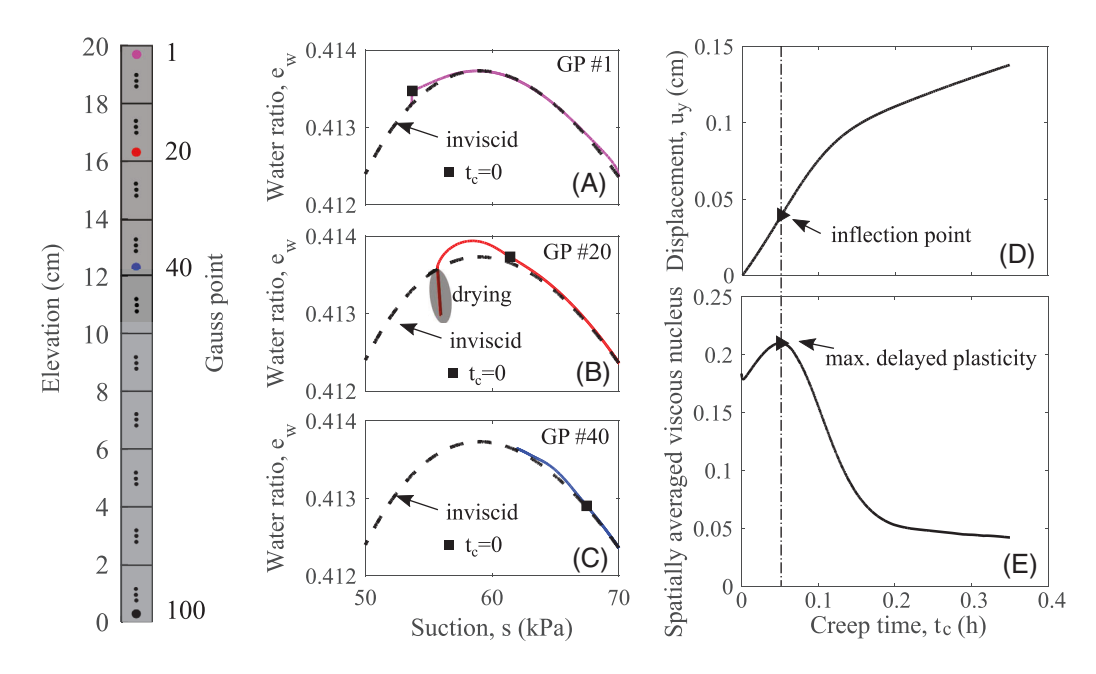


FIGURE 12 Creep responses under constant suction at the top surface: (A–C) relationship between suction and water ratio at selected Gauss points (#1, #20, and #40); (D,E) time histories of displacement and spatially averaged viscous nucleus of all Gauss points

introduced after water injection in the simulation based on a material with high hydraulic sensitivity. For this purpose, the nodal suction at the top of the column is fixed to a constant value after the end of the water injection stage (i.e., a stage of the analysis at which the sample is already undergoing post-instability conditions involving strain acceleration). As shown in Figures 11(A) and 12(A-C), after switching to suction control at the top surface, the water gradually permeates downwards, which saturates the underlying material but slightly dewaters the top surface. The advancing wetting front drives the propagation of the unstable zone since the saturation process causes more material elements to surpass the peak of e_w . Delayed plasticity sustained through viscous nucleus has the capacity to maintain the system acceleration right after the cessation of water injection until the spatially averaged viscous nucleus reaching its maximum value (Figures 12(D-E) and 13). However, without a continuous recharge of water flux through injection, time effects due to viscosity gradually fade away and the consolidation process starts to dominate the process bringing it to a new equilibrium condition. Consequently, the stabilizing effect of consolidation decelerates the system response and brings the unstable tertiary creep back to a stable primary creep. This example clearly illustrates the feedbacks controlling the global system

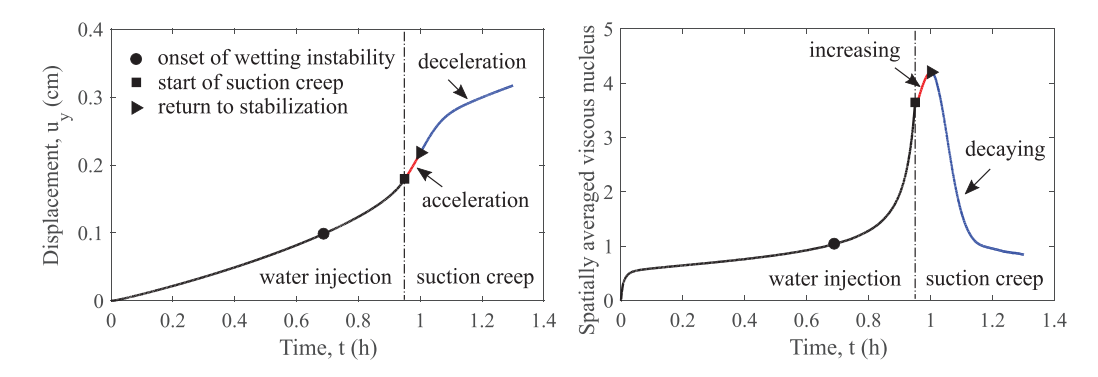


FIGURE 13 Time history of the global response: (A) displacement; (B) spatially averaged viscous nucleus

response, in which the local instability causes capillary suction loss and strain rate growth while competing with pore pressure diffusion, which mitigates the detrimental impacts of the wetting-induced instability, eventually suppressing them. It can therefore be concluded that the fate of a wet, collapsible soil mass in terms of post-failure movements can only be assessed by accounting for both the timescale of local material instability and the non-local diffusion of the resulting pore pressure transients.

5 | CONCLUSION

In this work, the field equation governing the fluid mass conservation of unsaturated soils has been mathematically examined to identify the connection between the criteria defining the loss of numerical stability and material failure due to wetting-induced weakening. By applying Darcy's law, the mass balance equation in terms of fluid pressure was formulated into a parabolic partial differential equation. Conditions defining the stability of the resulting PDE signify the illposedness of the coupled hydromechanical equations leading to a diffusive instability of the pore pressure transients. It was shown that such criterion shares similarities with the loss of controllability during water injection promoted by constitutive singularities. Consequently, it poses challenges to the numerical solution of coupled hydro-mechanical problems targeting unsaturated collapsible soils. Indeed, it has been shown that the onset of local failure of elastoplastic materials can trigger numerical ill-posedness, here manifested by the singularity of the discretized global operator of the coupled hydro-mechanical problem. To circumvent this problem, it was shown that a small amount of viscosity is sufficient to regularize the analysis and enhance the robustness of the algorithm, while maintaining a similar material response prior to failure. The difference in the treatment of plastic effects between elastoplasticity and viscoplasticity eventually modifies the mathematical characteristics of the governing equations. Unlike elastoplasticity, viscoplasticity treats the plastic effects as an additional source term contributing to the external forcing, thus removing its detrimental effects from the global stiffness matrix and suppressing the global singularity. These benefits enable material instability to be tracked through suitable indices specialized to unsaturated viscoplastic materials, which serve as a precursor of the rapid displacement accumulation and suction drop. Results from this work can therefore provide guidance to future investigations based on more general system configurations, hydro-mechanical forcing scenarios, and constitutive descriptions of soil inelasticity, that is, all essential factors for an accurate prediction of wetting-induced geohazards.

ACKNOWLEDGMENT

This study was financially supported by the U.S. National Science Foundation through grant ICER-1854951.

DATA AVAILABILITY STATEMENT

Data sharing not applicable to this article as no datasets were generated or analyzed during the current study.

ORCID



REFERENCES

- 1. Cascini L, Cuomo S, Guida D. Typical source areas of May 1998 flow-like mass movements in the Campania region, Southern Italy. *Eng Geol.* 2008:96(3–4):107–125.
- 2. Bekendam R, Pottgens J. Ground movements over the coal mines of southern Limburg, The Netherlands, and their relation to rising mine waters. *IAHS Publications-Series of Proceedings and Reports-Intern Assoc Hydrological Sciences*. 1995;234:3–12.
- 3. Alonso EE, Gens A, Josa A. A constitutive model for partially saturated soils. Géotechnique. 1990;40(3):405-430.
- 4. Buscarnera G, Nova R. An elastoplastic strain hardening model for soil allowing for hydraulic bonding–debonding effects. *Int J Numer Anal Methods Geomech.* 2009;33(8):1055–1086.
- 5. Mihalache C, Buscarnera G. Diffusive instability of pore pressure transients in deformable unsaturated soils. *J Eng Mech.* 2016;142(11):04016091.
- Garcia E, Oka F, Kimoto S. Instability analysis and simulation of water infiltration into an unsaturated elasto-viscoplastic material. Int J Solids Struct. 2010;47(25–26):3519–3536.
- 7. Buscarnera G, Di Prisco C. Discussing the definition of the second-order work for unsaturated soils. *Int J Numer Anal Methods Geomech*. 2012;36(1):36–49.
- 8. Buscarnera G, Nova R. Modelling instabilities in triaxial testing on unsaturated soil specimens. *Int J Numer Anal Methods Geomech*. 2011;35(2):179–200.
- 9. Imposimato S, Nova R. An investigation on the uniqueness of the incremental response of elastoplastic models for virgin sand. *Mechan Cohesive-Frictional Mater.* 1998;3(1):65–87.
- 10. Buscarnera G. Uniqueness and existence in plasticity models for unsaturated soils. Acta Geotech. 2014;9(2):313-327.
- 11. Buscarnera G, Dattola G, Di Prisco C. Controllability, uniqueness and existence of the incremental response: a mathematical criterion for elastoplastic constitutive laws. *Int J Solids Struct*. 2011;48(13):1867–1878.
- Mandel J. Conditions de stabilité et postulat de Drucker. In: Rheology and Soil Mechanics/Rhéologie et Mécanique des Sols, Springer, 1966, pp. 58–68.
- 13. Needleman A. Material rate dependence and mesh sensitivity in localization problems. *Comput Methods Appl Mech Eng.* 1988;67(1): 69–85.
- 14. Forest S, Lorentz E, et al. Localization phenomena and regularization methods. Local Approach Fract 2004;1:311-371.
- 15. Rice JR. On the stability of dilatant hardening for saturated rock masses. J Geophys Res. 1975;80(11):1531-1536.
- Vardoulakis I. Deformation of water-saturated sand: II. Effect of pore water flow and shear banding. Géotechnique. 1996;46(3):457–472.
- 17. Di Prisco C. A mathematical interpretation of the volumetric instability of loose sands. Comput Geotech. 1996;18(3):225-244.
- 18. Conti R, Tamagnini C, DeSimone A. Critical softening in Cam-Clay plasticity: adaptive viscous regularization, dilated time and numerical integration across stress-strain jump discontinuities. *Comput Methods Appl Mech Eng.* 2013;258:118–133.
- 19. Di Prisco C, Mancinelli L, Zanelotti L, Pisanò F. Numerical stability analysis of submerged slopes subject to rapid sedimentation processes. *Contin Mech Thermodyn.* 2015;27(1–2):157–172.
- 20. Ehlers W, Graf T, Ammann M. Deformation and localization analysis of partially saturated soil. *Comput Methods Appl Mech Eng.* 2004;193(27–29):2885–2910.
- 21. Mihalache C, Buscarnera G. Controllability criteria for soils saturated by a compressible fluid. J Eng Mech. 2016;142(10):04016076.
- 22. Coussy O. Poromechanics, John Wiley & Sons, 2004.
- 23. Romero E, Vaunat J. Retention curves of deformable clays. Experimental Evidence and Theoretical Approaches in Unsaturated Soils. 2000;91:106.
- 24. Romero E, Della Vecchia G, Jommi C. An insight into the water retention properties of compacted clayey soils. *Géotechnique*. 2011;61(4):313–328
- 25. Chen Y, Marinelli F, Buscarnera G. Mathematical interpretation of delayed instability in viscous unsaturated soil. Géotechn Lett. 2019:1-8.
- 26. Farlow SJ. Partial Differential Equations for Scientists and Engineers. Courier Corporation, 1993.
- 27. Li X. Effective stress in unsaturated soil: a microstructural analysis. Géotechnique. 2003;53(2):273–277.
- 28. Alonso EE, Pereira JM, Vaunat J, Olivella S. A microstructurally-based effective stress for unsaturated soils. *Géotechnique*. 2010;60(12):913–925.
- 29. Mihalache C, Buscarnera G. Is wetting collapse an unstable compaction process? J Geotech Geoenviron Eng. 2014;141(2):04014098.
- 30. Perzyna P. The constitutive equations for rate sensitive plastic materials. Q Appl Math. 1963;20(4):321–332.
- 31. Perzyna P. Fundamental problems in viscoplasticity. In: Advances in Applied Mechanics, vol 9. Elsevier; 1966:243–377.
- 32. Sloan SW. Substepping schemes for the numerical integration of elastoplastic stress-strain relations. *Int J Numer Methods Eng.* 1987;24(5):893–911.
- 33. Sheng D, Sloan SW, Gens A, Smith DW. Finite element formulation and algorithms for unsaturated soils. Part I: theory. *Int J Numer Anal Methods Geomech.* 2003;27(9):745–765.
- 34. Zienkiewicz OC, Chan A, Pastor M, Schrefler B, Shiomi T. Computational Geomechanics, Citeseer, 1999.
- 35. Mihalache C. A Comprehensive Strategy for the Assessment of Stability Conditions in Porous Media at Varying Levels of Water Saturation, Ph.D. thesis, Northwestern University, 2016.
- 36. Mira P, Benítez A, Pastor M, Merodo JF. A new incompatible mode element with selective mass scaling for saturated soil dynamics. *Acta Geotech.* 2018;13(2):267–282.

- 37. Liakopoulos AC. Transient flow through unsaturated porous media, Ph.D. thesis, University of California, Berkeley, 1964.
- 38. Van Genuchten MT. A closed-form equation for predicting the hydraulic conductivity of unsaturated soils 1. Soil Sci Soc Am J. 1980;44(5):892–898.
- 39. Mualem Y. A conceptual model of hysteresis. Water Resour Res. 1974:10(3):514-520.
- 40. Sekiguchi H. Theory of undrained creep rupture of normally consolidated clay based on elasto-viscoplasticity. *Soils Found*. 1984;24(1):129–147
- 41. Leong W, Chu J. Effect of undrained creep on instability behaviour of loose sand. Can Geotech J. 2002;39(6):1399-1405.
- 42. Nicot F, Darve F, Khoa HDV. Bifurcation and second-order work in geomaterials. *Int J Numer Anal Methods Geomech.* 2007;31(8):1007–1032.
- 43. Nicot F, Challamel N, Lerbet J, Prunier F, Darve F. Some insights into structure instability and the second-order work criterion. *Int J Solids Struct*. 2012;49(1):132–142.
- 44. Nicot F, Lerbet J, Darve F. Second-order work criterion: from material point to boundary value problems. *Acta Mech.* 2017;228(7):2483–2498
- 45. Zhao CF, Yin ZY, Hicher PY. A multiscale approach for investigating the effect of microstructural instability on global failure in granular materials. *Int J Numer Anal Methods Geomech.* 2018;42(17):2065–2094.
- 46. Malet JP, Maquaire O, Locat J, Remaître A. Assessing debris flow hazards associated with slow moving landslides: methodology and numerical analyses. *Landslides*. 2004;1(1):83–90.
- 47. Sloan SW, Abbo AJ. Biot consolidation analysis with automatic time stepping and error control Part 1: theory and implementation. *Int J Numer Anal Methods Geomech.* 1999;23(6):467–492.
- 48. Zienkiewicz OC, Cormeau IC. Visco-plasticity and creep in elastic solids—a unified numerical solution approach. *Int J Numer Methods Eng.* 1974;8(4):821–845.
- 49. Laloui L, Klubertanz G, Vulliet L. Solid-liquid-air coupling in multiphase porous media. *Int J Numer Anal Methods Geomech*. 2003;27(3):183–206.
- 50. Hu R, Chen Y, Zhou C. Modeling of coupled deformation, water flow and gas transport in soil slopes subjected to rain infiltration. *Sci China Technol Sci.* 2011;54(10):2561.
- 51. Khoei A, Mohammadnejad T. Numerical modeling of multiphase fluid flow in deforming porous media: a comparison between two-and three-phase models for seismic analysis of earth and rockfill dams. *Comput Geotech.* 2011;38(2):142–166.
- 52. Ju J. Consistent tangent moduli for a class of viscoplasticity. J Eng Mech. 1990;116(8):1764-1779.
- Pisanò F, Di Prisco C. A stability criterion for elasto-viscoplastic constitutive relationships. Int J Numer Anal Methods Geomech. 2016;40(1):141–156.

How to cite this article: Chen Y, Buscarnera G. Numerical simulation of unstable suction transients in unsaturated soils: the role of wetting collapse. *Int J Numer Anal Methods*. 2021;45:1569–1587. https://doi.org/10.1002/nag.3214

APPENDIX A

A.1 Loss of controllability of wetting paths in elastoplastic materials

According to the controllability theory, the stability index \mathcal{H} for elastoplastic materials for a given testing condition can be derived from the consistency function by replacing the unknowns with the controlled variables. Specifically, for the wetting test under prescribed suction and constant stress, the stability index can be customized by replacing $\sigma'_{ij,t}$ in Equation 10 by $\sigma^{\text{net}}_{ij,t}$, which comes:

$$\Lambda = \frac{1}{H} \left[\frac{\partial f}{\partial \sigma'_{ij}} \sigma_{ij,t}^{\text{net}} + \left(\frac{\partial f}{\partial \sigma'_{ij}} \frac{\partial \sigma'_{ij}}{\partial s} + \frac{\partial f}{\partial \sigma_{y}} \frac{\partial \sigma_{y}}{\partial s} \right) s_{,t} \right]$$
(A.1)

In this context, the stability index \mathcal{H} for suction-controlled wetting test is defined as:

$$\mathcal{H} = H \tag{A.2}$$

While for the wetting test under prescribed water injection and constant stress, the stability index can be customized by replacing $\sigma'_{ij,t}$ and $s_{,t}$ in Equation (10) by $\sigma^{\text{net}}_{ij,t}$ and $e_{w,t}$. For this purpose, it first combines Equations (8) with (9) to

formulate the suction increment s_t in terms of the controlled variables:

$$s_{,t} = \frac{1}{B} \left(\frac{e_{w,t}}{1+e} + S_r C_{ijkl}^e \sigma_{ij,t}^{\text{net}} \delta_{kl} + S_r \Lambda \frac{\partial g}{\partial \sigma'_{ij}} \delta_{ij} \right)$$
(A.3)

And then, inserting Equations 2 and A.3 into Equation 10, it obtains:

$$\Lambda = \frac{1}{H - H_{\chi}} \left[\frac{\partial f}{\partial \sigma'_{ij}} \sigma_{ij,t}^{\text{net}} + \frac{1}{B} \left(\frac{\partial f}{\partial \sigma'_{ij}} \frac{\partial \sigma'_{ij}}{\partial s} + \frac{\partial f}{\partial \sigma_{y}} \frac{\partial \sigma_{y}}{\partial s} \right) \left(\frac{e_{w,t}}{1 + e} + S_{r} C_{ijkl}^{e} \sigma_{ij,t}^{\text{net}} \delta_{kl} \right) \right]$$
(A.4)

Therefore, the stability index \mathcal{H} for water injection tests under constant stress is proved to be:

$$\mathcal{H} = H - H_{\gamma} \tag{A.5}$$

where H and H_χ take the same form as defined in Equations 12 and 14, respectively.

A.2 | Numerical discretization of the field equations

The field equations governing the coupled hydromechanical process for elastoplastic and viscoplastic unsaturated porous media are discretized and solved through a finite element (FE) method. Based on the standard FE approach,⁴⁷ the continuity equation of the fluid flow formulated in Equation (3) can be converted as:

$$\mathbf{L}'\dot{\mathbf{U}} + \mathbf{W}\dot{\mathbf{P}} + \mathbf{H}\mathbf{P} = \dot{\mathbf{Q}}_{\text{ext}} \tag{A.6}$$

with:

$$\mathbf{L}' = \sum \int_{V} \mathbf{N}_{w}^{T} S_{r} \delta^{T} \mathbf{B}_{u} dV$$

$$\mathbf{W} = \sum \int_{V} \mathbf{N}_{w}^{T} n \frac{\partial S_{r}}{\partial s} \delta \mathbf{N}_{w} dV$$

$$\mathbf{H} = \sum \int_{V} \mathbf{B}_{w}^{T} \frac{\mathbf{k}^{w}}{\gamma_{w}} \mathbf{B}_{w} dV$$

$$\dot{\mathbf{Q}}_{\text{ext}} = -\sum \int_{S} \mathbf{N}_{w}^{T} \mathbf{q}^{w} dS - \sum \int_{V} \mathbf{B}_{w}^{T} \frac{\mathbf{k}^{w}}{\gamma_{w}} \mathbf{b}_{w} dV$$
(A.7)

where V is the volume of the domain, S is the area of the prescribed traction boundary, \mathbf{q}^w is a vector of the prescribed fluid flux, \mathbf{b}_w is the body force vector for the fluid phase, \mathbf{N}_w is the shape function for the pore fluid pressure field, \mathbf{P} is the vector of nodal pore pressures, and \mathbf{N}_u and \mathbf{B}_u are the matrices of shape function and its time derivative in the displacement field, defined as:

$$\dot{u} = \mathbf{N}_{u}^{\mathrm{T}} \dot{\mathbf{U}}, \dot{\varepsilon} = \mathbf{B}_{u}^{\mathrm{T}} \dot{\mathbf{U}} \tag{A.8}$$

in which U denotes the vector of the nodal displacement and u and ε are the displacement and strain field at a given location. Without consideration of the dynamic effect due to slow loading rate, the momentum equilibrium can be expressed as⁴⁷:

$$\int_{V} \mathbf{B}_{u}^{\mathrm{T}} \dot{\boldsymbol{\sigma}} dV - \int_{S} \mathbf{N}_{u}^{\mathrm{T}} \dot{\boldsymbol{t}} dS - \int_{V} \mathbf{N}_{u}^{\mathrm{T}} \dot{\boldsymbol{b}} dV = \mathbf{0}$$
(A.9)

where **b** is the body force vector, **t** is a vector of external surface traction. The different mathematical structure of elastoplasticity and viscoplasticity requires separate treatments of constitutive laws which eventually impacts the property of the coupled hydro-mechanical solver. Specifically, for elastoplastic materials, the constitutive relationship under unsaturated

conditions can be generalized as4:

$$\dot{\boldsymbol{\sigma}}' = \mathbf{D}^{\sigma\sigma}\dot{\boldsymbol{\varepsilon}} - \mathbf{D}^{\sigma w}\dot{\boldsymbol{s}}$$

$$\mathbf{D}^{\sigma\sigma} = \mathbf{D}^{e} - \frac{1}{H - H_{c}} \left(\mathbf{D}^{e} \frac{\partial g}{\partial \boldsymbol{\sigma}'} \right) \otimes \left(\frac{\partial f}{\partial \boldsymbol{\sigma}'} \mathbf{D}^{e} \right)$$

$$\mathbf{D}^{\sigma w} = \frac{1}{H - H_{c}} \frac{\partial f}{\partial \sigma_{v}} \frac{\partial \sigma_{y}}{\partial \boldsymbol{s}} \mathbf{D}^{e} \frac{\partial g}{\partial \boldsymbol{\sigma}'}$$
(A.10)

where the critical hardening modulus H_c is expressed as:

$$H_c = -\frac{\partial f}{\partial \sigma'} \mathbf{D}^e \frac{\partial g}{\partial \sigma'} \tag{A.11}$$

By inserting Equations (2) and (A.10) into (A.9), it obtains:

$$\mathbf{K}^{ep}\dot{\mathbf{U}} + \mathbf{L}^{ep}\dot{\mathbf{P}} = \dot{\mathbf{F}}^{ep}_{\text{out}} \tag{A.12}$$

with

$$\mathbf{K}^{ep} = \sum \int_{V} \mathbf{B}_{u}^{\mathrm{T}} \mathbf{D}^{\sigma\sigma} \mathbf{B}_{u} dV,$$

$$\mathbf{L}^{ep} = \sum \int_{V} \mathbf{B}_{u}^{\mathrm{T}} \left[\mathbf{D}^{\sigma w} + \left(S_{r} + s \frac{\partial S_{r}}{\partial s} \right) \delta \right] \mathbf{N}_{w} dV$$

$$\dot{\mathbf{F}}_{\text{ext}}^{ep} = \sum \int_{S} \mathbf{N}_{u}^{\mathrm{T}} \dot{\mathbf{t}} dS + \sum \int_{V} \mathbf{N}_{u}^{\mathrm{T}} \dot{\mathbf{b}} dV$$
(A.13)

While unlike elastoplastic materials, the use of a viscoplastic flow rule based on the overstress implies:

$$\dot{\sigma}' = \mathbf{D}^e \dot{\varepsilon} - \phi \mathbf{D}^e \frac{\partial g}{\partial \sigma'} \tag{A.14}$$

By inserting Equation (A.14) into Equation (A.9), it follows 48 :

$$\mathbf{K}^{vp}\dot{\mathbf{U}} + \mathbf{L}^{vp}\dot{\mathbf{P}} = \dot{\mathbf{F}}_{\text{ext}}^{vp} \tag{A.15}$$

with

$$\mathbf{K}^{vp} = \sum \int_{V} \mathbf{B}_{u}^{T} \mathbf{D}^{e} \mathbf{B}_{u} dV$$

$$\mathbf{L}^{vp} = \sum \int_{V} \mathbf{B}_{u}^{T} \left(S_{r} + s \frac{\partial S_{r}}{\partial s} \right) \delta \mathbf{N}_{w} dV$$

$$\dot{\mathbf{F}}_{\text{ext}}^{vp} = \dot{\mathbf{F}}_{\text{ext}}^{ep} + \dot{\mathbf{F}}_{\text{ext}}^{ps}, \dot{\mathbf{F}}_{\text{ext}}^{ps} = \sum \int_{V} \mathbf{B}_{u}^{T} \phi \mathbf{D}^{e} \frac{\partial g}{\partial \sigma'} dV$$
(A.16)

A.3 | Validation of the numerical implementation

The numerical implementation can be validated through the Liakopoulos drainage test,³⁷ a benchmark widely used for the verification of multi-phase coupled models. In the experiment, a fully saturated sand column with 1 m in height was tested and a high-permeability sandstone was placed at the bottom of the soil column to allow vertical drainage under gravity, while an impermeable cylinder was used on the lateral surface. Such a drainage process is here simulated with the

TABLE A.1 Model parameters of the Liakopoulos drainage test

E [kPa]	$a_v g$	$m_v g$	$n_v g$	$k^{\rm sat}$ [m/s]
13000	0.04	1.03	2.5	4.4e-6

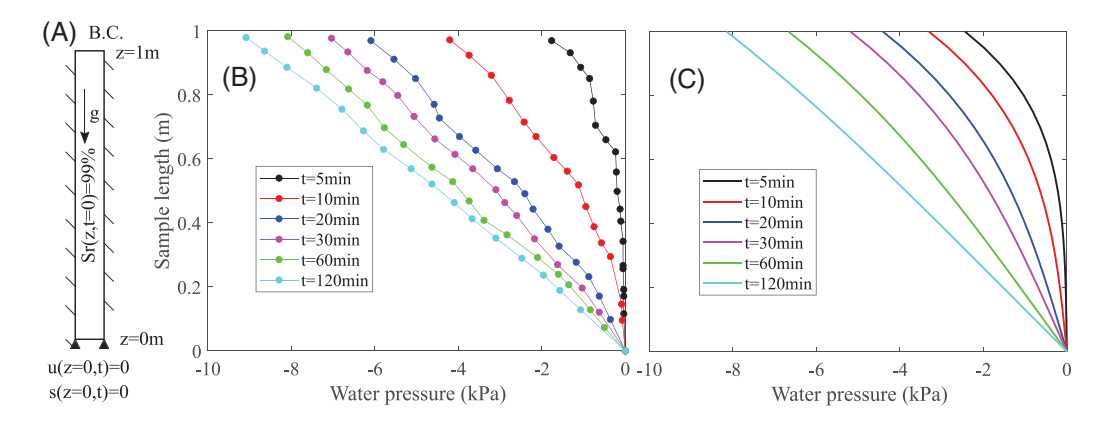


FIGURE A.1 Pore water pressure distribution of the Liakoupoulos drainage test: (A) Boundary condition (B.C.); (B) experiment; (C) simulation

numerical model discussed in this paper. Due to the lack of measurements of mechanical properties, linear elasticity is used in conjunction with a Young's modulus of 13,000 kPa,²⁰ while the soil water retention characteristics are calibrated based on reported data. The model parameters are listed in Table A.1 and the initial and boundary conditions are described in Figure A.1(a). Specifically, an initial degree of saturation of 99% is applied uniformly throughout the sample to avoid numerical problems caused by the transition from full to partial saturation.⁴⁹ As shown in Figure A.1(b) and (c), the simulations satisfactorily capture the evolution of the pore water pressure across the column. Minor mismatches exist due to the simplified nature of the model, but can in principle be mitigated through an explicit simulation of the pore air phase.^{50,51} Nevertheless, the example shows that the performance of the selected numerical approach is satisfactory both in terms of its numerical accuracy and of its realistic representation of fundamental hydro-mechanical processes in unsaturated soils.

A.4 Loss of controllability of wetting paths in viscoplastic materials

Since viscoplastic models do not enforce plastic consistency conditions,⁵² standard controllability criteria based on tangent constitutive operators cannot be used. Recent work by Pisano and di Prisco⁵³ offered a theoretical framework to interpret the viscoplastic stability, which requires the second-order time derivative of response variables summarized by the following ordinary differential equations:

$$\dot{\mathbf{X}} = \mathbf{A}\mathbf{X} + \mathbf{F} \tag{A.17}$$

where vectors \mathbf{X} and $\dot{\mathbf{X}}$ contain the rates of response variables and their acceleration, \mathbf{F} is a forcing term related to the imposed controls being zero during creeping, and \mathbf{A} is a constitutive operator. The presence of positive eigenvalues of \mathbf{A} signifies a diverging response and the system tends to accelerate. Particularly, stability condition of wetting processes can be mathematically represented by the strain acceleration, 25 formulated as:

$$\ddot{\varepsilon}_{ij} = A\dot{\varepsilon}_{ij} + F_{ij} \tag{A.18}$$

and the stability index is expressed as:

$$A = -\frac{\partial \phi}{\partial f} \mathcal{H}^{\upsilon} \frac{B}{n} \frac{\partial s}{\partial S_r} + \phi \frac{\partial^2 g}{\partial \sigma'_{ij} \partial \sigma'_{kl}} \frac{\partial \sigma'_{ij}}{\partial S_r} \frac{S_r}{n} \delta_{kl}$$
(A.19)

WILEY 1587

in which:

$$\mathcal{H} = H - H_{\chi} - \frac{H_{\sigma_{ij}^{\text{net}}} + H_{e_w}}{\phi}$$

$$H_{\sigma_{ij}^{\text{net}}} = \left[\frac{\partial f}{\partial \sigma_{ij}'} + \frac{S_r}{B} \left(\frac{\partial f}{\partial \sigma_{ij}'} \frac{\partial \sigma_{ij}'}{\partial s} + \frac{\partial f}{\partial \sigma_y} \frac{\partial \sigma_y}{\partial s} \right) C_{ijkl}^e \delta_{kl} \right] \sigma_{ij,t}^{\text{net}}$$

$$H_{e_w} = \frac{1}{B} \left(\frac{\partial f}{\partial \sigma_{ij}'} \frac{\partial \sigma_{ij}'}{\partial s} + \frac{\partial f}{\partial \sigma_y} \frac{\partial \sigma_y}{\partial s} \right) \frac{e_{w,t}}{1 + e}$$
(A.20)

It is apparent that during water-undrained creep (i.e., $\dot{\sigma}^{\rm net}=0$ and $\dot{e}_w=0$), $H_{\sigma^{\rm net}_{ij}}$ and H_{e_w} approach zero. For relatively simple constitutive laws (i.e., those characterized by a homothetic plastic potential, such as Cam-clay model), the second-order terms in A vanishes and the stability condition is solely governed by the term $H-H_\chi$, leading to the transition from stable to unstable creep always being located in the proximity of the underlying rate-independent failure.